01,11

XXI All-Russian School-Seminar on Problems of Condensed Matter Physics (SPCMP-21), Ekaterinburg, March 18-25, 2021.

In situ TEM study of phase transformations in nonstoichiometric $Ni_{46}Mn_{41}In_{13}$ Heusler alloy

© D.D. Kuznetsov[1], E.I. Kuznetsova[2], A.V. Mashirov[1], A.S. Loshachenko[3], D.V. Danilov[3], G.A. Shandryuk[4], V.G. Shavrov[1], V.V. Koledov[1]

[1] Kotelnikov Institute of Radio Engineering and Electronics, Russian Academy of Sciences, Moscow, Russia
[2] M.N. Mikheev Institute of Metal Physics, Ural Branch, Russian Academy of Sciences, Yekaterinburg, Russia
[3] IRC Nanotechnology, Research Park, St. Petersburg State University, St. Petersburg, Russia
[4] Topchiev Institute of Petrochemical Synthesis, Russian Academy of Sciences, Moscow, Russia

E-mail: kuznetsov.dmitry89@gmail.com

Received July 8, 2021
Revised July 8, 2021
Accepted July 8, 2021

This paper presents a study of the metamagnetostructural transition of the martensitic type in the $Ni_{46}Mn_{41}In_{13}$ alloy with magnetic shape memory and inverse magnetocaloric effect. The characteristic temperatures of the direct transition starting $M_s = 253$ K and its finishing $M_f = 164$ K, as well as the reverse temperatures $A_s = 203$ K and $A_f = 236$ K, respectively, were determined by differential scanning calorimetry. The characteristic peculiarities of the transition: a decrease of the Ms and the presence of a residual austenite phase, as well as pre-martensitic states, were studied using transmission electron microscopy. The estimated the thickness of alloy was 50 nm, when martensitic transition suppressed.

Keywords: martensitic transformation, metamagnetostructural transformation, premartensitic states.

DOI: 10.21883/PSS.2022.13.52296.10s

1. Introduction

In recent years, Heusler alloys of the Ni-Mn-Z (Z = Ga, In, Sn) systems are of great interest of the researchers, as ferromagnetic alloys with the shape memory effect (SME) caused by unique physical properties and their potential application for creation of magnetic actuators, spintronic devices and solid-state magnetic cooling systems [1–7].

Ni-Mn-In system-based alloys are a class of materials demonstrating the effect of magnetic shape memory accompanying martensite transformation from the cubic phase (austenite) to low-symmetry phase (martensite). Regardless of intensive studies, the mechanism of martensite transformation in that system still remains unclear to some extent. So called pre-transient phenomena are observed in the alloys capable of undergoing martensite transformation, in which metastable pre-martensite phase is considered as a precursor of thermodynamically stable martensite phase. At the same time, the material demonstrates an anomaly of elastic, thermal, electrical and magnetic properties. These anomalies are directly related with evolution of the pre-martensite structure, which can be considered as infant martensite phase or, as an actually independent phase before martensite transformation, which is indicated by the studies of the Ti-Ni-based alloys [8].

Pre-martensite phase in the Ni-Mn-In system preserves general cubic symmetry of original high-temperature austenite phase $L2_1$, but, as shown by electron-microscope studies, it is a complex state in the nanometer scale, with formation of a thin regular structure called tweed. Tweed contrast is observed in many alloys demonstrating transformation according to the martensite type, compounds based on Y-Ba-Cu-O and other Heusler alloys [9–11]. Many today's explanations of the anomalies of pre-martensite phenomena, including tweed structure, are based on the effects associated with the composition fluctuations and chemical delamination, which cause the lattice deformation state [12]. Khachaturian et al assume, that pre-martensite tweed structure results from coherent nanodisperse emissions built-into original phase at the initial degradation stage, and, subject to that, they suggest a concept „of pseudospinodal decomposition" [13]. In recent time, these ideas are being revised subject to new theoretical approaches and experimental results [14].

Moreover, in recent time, many studies have concentrated on the research of so called „dimension effects", which play

key role in suppression of the martensite transformation process [15]. The authors of the work [16] established that in the nanostructured Ni-Ti thermally-induced martensite transformation is fully suppressed with the grain size below 50 nm. Similar study in thin Ni-Ti films has shown that martensite transformation is suppressed, when the film thickness is reduced to 50 nm [17].

This work studied peculiarities of metamagnetic martensite transformation of the alloy $Ni_{46}Mn_{41}In_{13}$ in thin V-shaped foil. Pre-martensite effects were studied, and the impact of magnetic field and thickness of foil to the temperature of martensite transformation.

2. Samples and experimental procedure

Polycrystalline samples of the alloy $Ni_{46}Mn_{41}In_{13}$ as ingots with the weight about 30 g were produced from high-purity raw metals Ni, Mn, In (99.99%) by arc melting method in argon atmosphere on a cold bed with three turns around and meltdowns. For the purpose of homogenization, the ingots annealing was done in the vacuum at the temperature of 900°C during 24 hours with further slow cool down in the furnace to the room temperature.

Typical temperatures of the beginning and finish of direct and reverse metamagnetic structural transformation, and the Curie temperature were determined by the method of differential scanning calorimetry (DSC) by means of the instrument METTLER TOLEDO DSC3$^+$ within the temperature interval from −173 to 327°C.

The field dependencies of the magnetization intensity of the sample on the temperature were checked by means of VersaLab magnetometer „Quantum Design“ in the fields 1 T, 2 T, 3 T according to the following protocol: zero field cooling (ZFC); field cooling (FC); field heating (FH) in the temperature interval from 50 to 400 K.

Crystalline structure of the sample was studied in the temperature range 100−340 K by means of the transmission electron microscope (TEM) Carl Zeiss Libra 200FE (accelerating voltage 200 kV) with energetic OMEGA filter, energy disperse detector of X-ray emissions Oxford Instruments X-Max 80 and double-axis cryoanalytical holder Gatan Model 636 with the temperature controller Model 900 SmartSet cold stage controller.

Electron-microscope studies were done on foils produced by standard methods in light- and dark-field modes of making the images. Microdiffraction method was used for identification of local phases. For direct determination of the foil thickness, after performance of microscopic studies, a cut was made in the studied location by means of focused ion-beam Ga at a double-beam workstation Carl Zeiss Auriga Laser.

Electron-microscope studies and preparation of foils for TEM were made in the Interdisciplinary resource center for the field of „Nanotechnologies“, of Saint Petersburg State University, Saint Petersburg. „Nanotechnologies“, Shared Use Center Research Park of the Saint Petersburg State University, city of Saint Petersburg.

3. Results discussion

The temperatures of the beginning and finish of direct (M_s and M_f) and reverse (A_s and A_f) metamagnetic structural transformations, as well the Curie temperature (T_c): $M_s = 253$ K, $M_f = 164$ K, $A_s = 203$ K, $A_f = 236$ K, $T_c = 323$ K (during cooldown from the austenite phase) and 329 K (during heating from the martensite phase) were determined by using DSC method. Thermogram is shown in Fig. 1.

The data of field dependencies of the magnetization intensity show that the material sensitivity to the magnetic field was $K_{Ms} = 7$ K/T (Fig. 2), i.e. applicable external magnetic fields shift the temperature of metamagnetic structural transformation by 7 K to the low temperatures end.

The dependence was found for the temperature of beginning of the metamagnetic structural transformation of the martensite type on the thickness of sample in the form of V-shaped foil. It was found, that the martensite phase in case of direct martensite transformation, within thin area of foil with the thickness below 150 nm, begin to appear at $M_s = 215$ K (i.e. at the temperatures below that in a thick material) after the first cycle of cool down–heating–cool down, after the second cycle $M_s = 210$ K and after the third cycle $M_s = 208$ K, this, probably, is associated with accumulation of defects and/or oxidation of the material; this phenomenon requires a separate study. Further temperature decrease for each of cycles results in increase of the martensite portion, however, the transformation is blocked at the distance of about 600 nm from the sample edge with the plate thickness below 50 nm, therefore, no martensite structure formation is observed there even at the temperature of liquid nitrogen (Fig. 3).

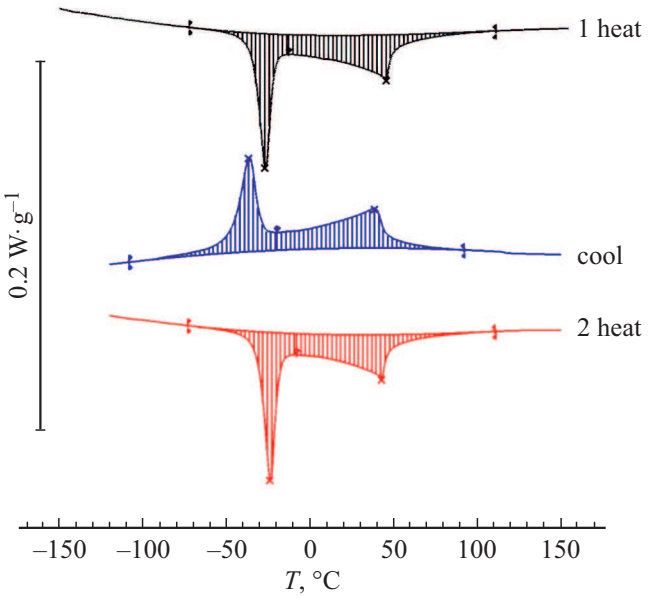

Figure 1. Thermogram for the alloy $Ni_{46}Mn_{41}In_{13}$: 1 heat — measurement at the first heating from −173 to 327°C; cool — measurement during cool down from 327 to −173°C; 2 heat — measurement at the second heating from −173 to 327°C.

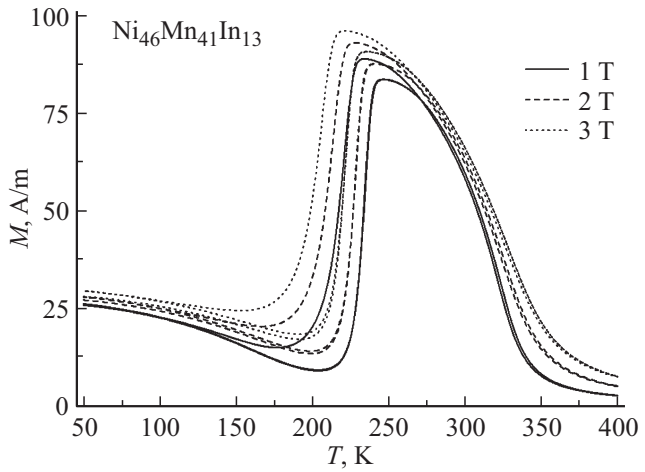

Figure 2. Graph of dependence of the sample magnetization intensity (M (A/m)) on the temperature (T (K)).

Since the observed phenomena have some perspectives due to potential application of the studied alloy in the nanoscale devices, the study of peculiarities of the martensite transformation in thin V-shaped foil seems to be of a high interest. Impact of „dimension effects“ to main parameters characterizing the martensite transformation, such as M_s, are generally considered in terms of availability of energy barriers associated with the energy of the boundaries of austenite–martensite and martensite–martensite, which decelerate or even completely block the transformation [16]. Moreover, the laws of reformation during martensite transformation arise from orientation ratios between atomic-crystalline lattices of austenite and martensite phases and their microstructural peculiarities. Given the structure of non-stoichiometric alloys based on the Ni-Mn-In compound is less studied, than the structure of stoichiometric compound, we consider in detail the evolution of thin structure of the alloy $Ni_{46}Mn_{41}In_{13}$.

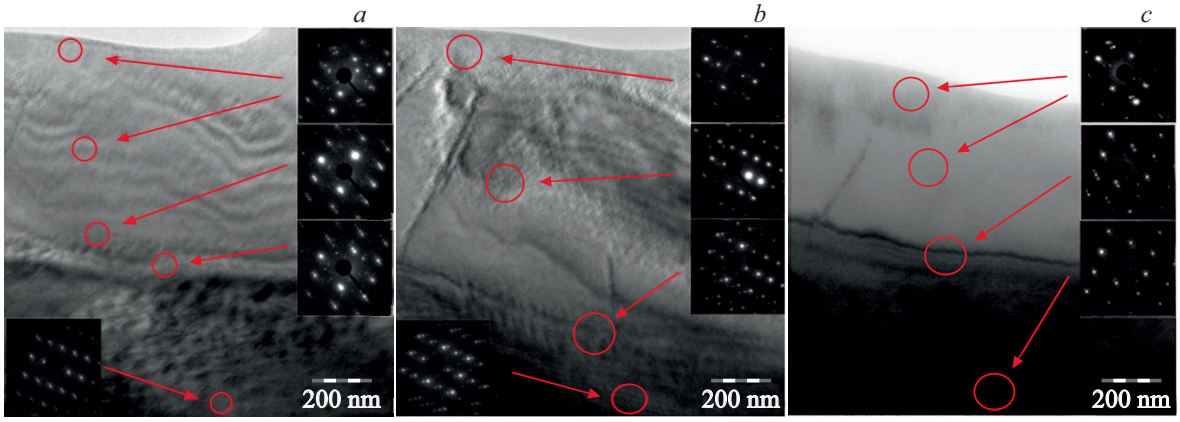

Figure 3. Light-field images and diffraction pictures of the highlighted locations of the alloy $Ni_{46}Mn_{41}In_{13}$ at the temperature 215 K (a), 208 K (b), 100 K (c).

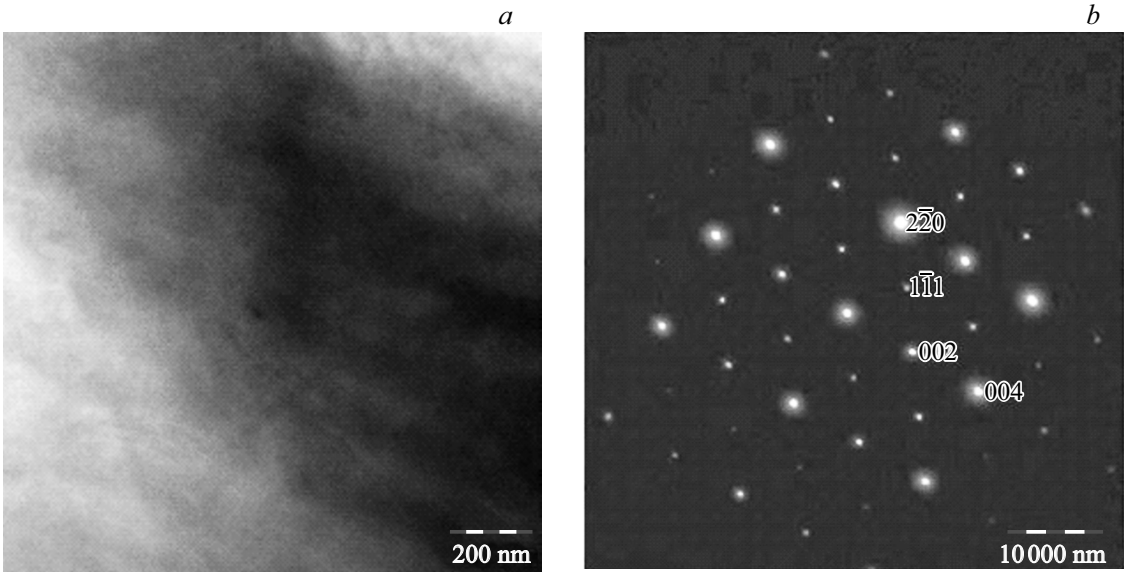

Figure 4. Microstructure of the austenite phase of the alloy $Ni_{46}Mn_{41}In_{13}$: a — light-field image; b — electron-diffraction pattern, axis of the area $[110]_{L21}$.

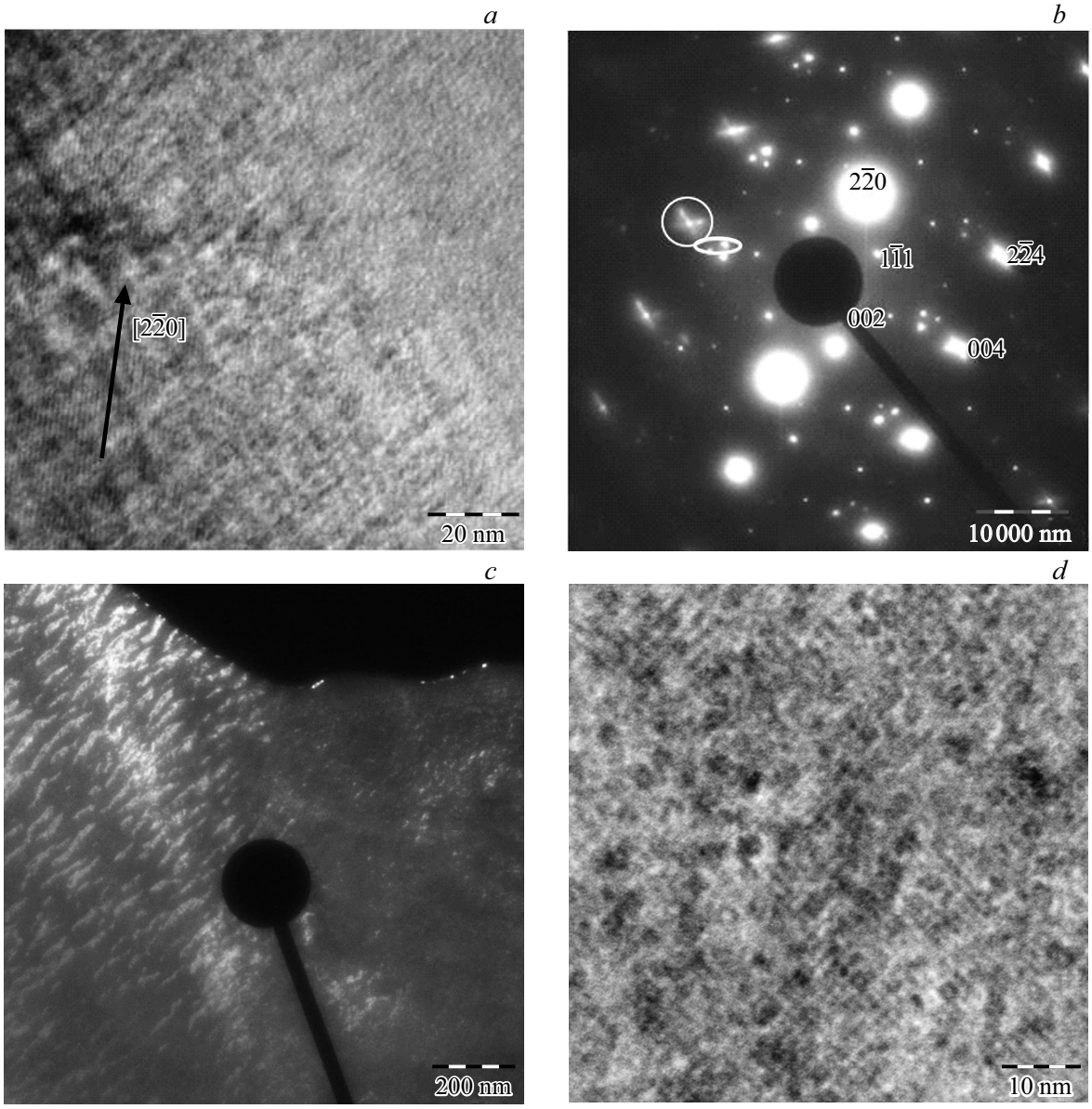

Figure 5. Microstructure of the alloy $Ni_{46}Mn_{41}In_{13}$: *a* — bright-field image; *b* — electron-diffraction pattern, axis of the area $[110]_{L21}$; *c* — dark-field image in reflex outlined with ellipse on the electron-diffraction pattern; *d* — bright-field image at higher magnification.

Austenite. Fig. 4 shows the structure of austenite (Fig. 4, *a* — bright-field image) of the phase of the studied alloy $Ni_{46}Mn_{41}In_{13}$.

Microdiffraction picture (Fig. 4, *b*) corresponds to one of the possible variants of the axis of the area [110] of austenite with the lattice $L2_1$ ($a = 6.17$ Å). The presence of (111) of superstructural reflexes indicates a good ordered phase $L2_1$ in that system. The observed tweed contrast (Fig. 5, *a*) is accompanied by certain type of diffusion scattering (circled in Fig. 5, *b*). The distance between the bands of tweed structure is 5–10 nm. In the left part of Fig. 5, *a* there is additional contrast — long thin stipes parallel to the plane (220). The distance between the stripes is about 1.2 nm, which corresponds to six distances between the planes (220). In dark-field image (Fig. 5, *c*) obtained in two of three reflexes (highlighted with ellipse in Fig. 5, *b*), there is a modulated structure of other type. This structure is like a classical modulated structure of concentration type created by the fields of stresses indicating local distortions of the lattice. Since the modulated martensite structure is created by periodic displacement of the plane (110) in direction of ⟨110⟩ of austenite phase or the plane (112) in direction of ⟨111⟩ of austenite phase, pre-transient phenomena represent shifts of atoms to the future phase. Atom shifts from the equilibrium positions cause deformations of the lattice, which appear as modulated structures, in particular, as tweed microstructure. Such tweed domains appearing in the pre-martensite state,

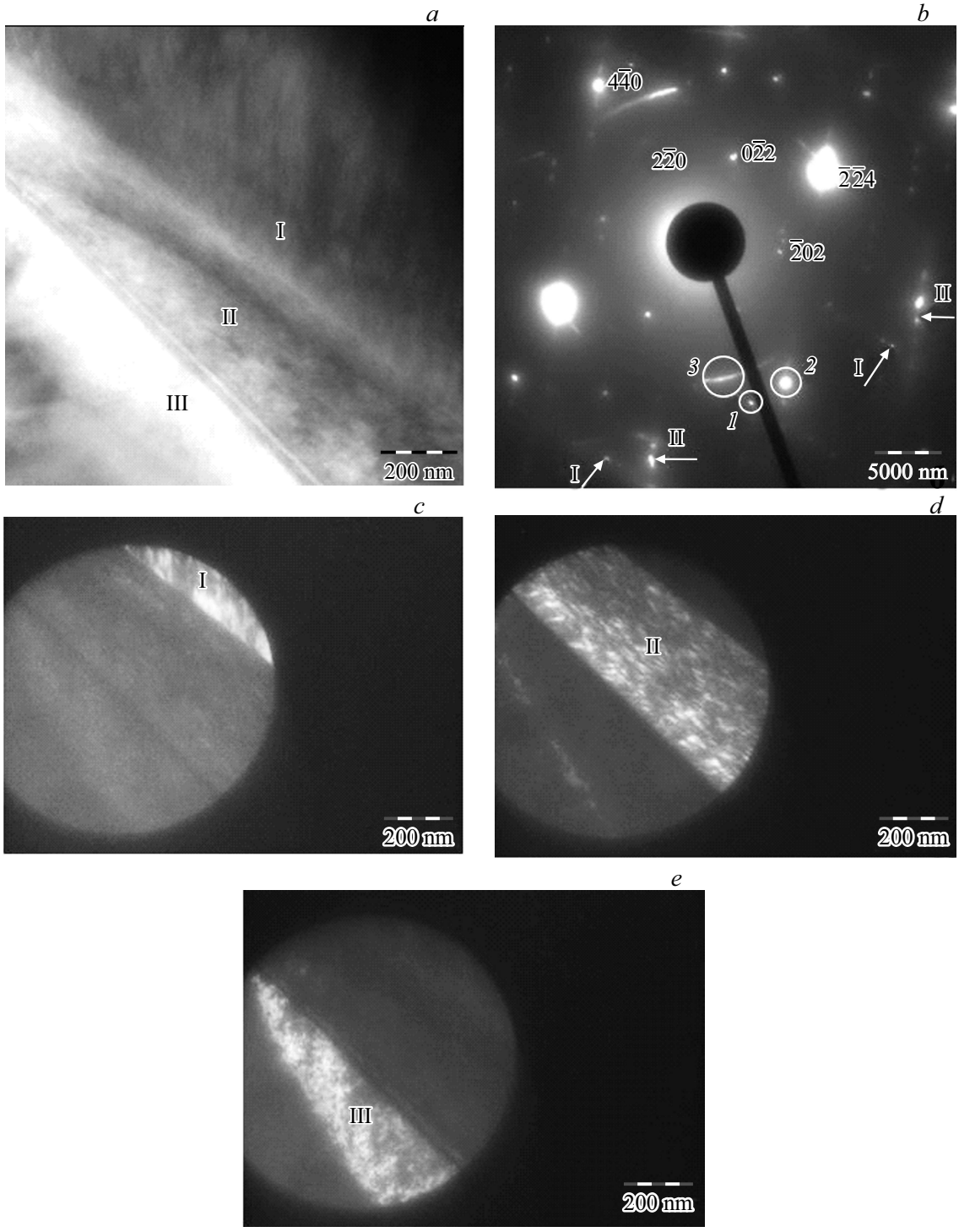

Figure 6. Microstructure of the alloy $Ni_{46}Mn_{41}In_{13}$: *a* — bright-field image; *b* — electron-diffraction pattern, axis of the area $[111]_{L21}$; *c* — dark-field image in reflex 1; *d* — dark-field image in reflex 2; *e* — dark-field image in azimuth fuzzy reflex 3.

probably, are the places of martensite generation. At the same time, satellites and typical diffusion scattering appear in diffraction pictures.

In a non-stoichiometric alloy there can be the processes of concentration delamination accompanied by emission of nanodisperse particles that are coherent or partly coherent to the matrix. This, in turn, will result in internal stresses and occurrence of black-white and tweed contrast. In Fig. 5, *d*, obtained at a high magnification, there are nanodimension (about 2–3 nm) evenly distributed emissions, which are clearly distinguished on the tweed contrast background. Such a contrast, in the form of domain

structure, was observed as a result of low-temperature spinodal decomposition of non-stoichiometric compound $YBa_2Cu_3O_{7-\delta}$ and was caused by emission of particles of the oxygen-rich orthophase in the oxygen-depleted matrix [18].

Co-existence of austenite and martensite. Fig. 6 and 7 show microimages and diffraction pictures from the austenite areas and the areas that undergone martensite transformation. Fig. 6, *a* represents a structure consisting of two laminar crystals of martensite. According to the observed orientations of striped contrast inside the martensite crystals, and directions of the rows of reflexes on the electron-diffraction patterns corresponding to it (shown by arrows in Fig. 6, *b*), one may conclude on the presence of two different orientations of martensite designated by I and II. Comparison of dark-field and bright-field images and their comparison to relevant electron-diffraction patterns shows that one system of reflexes belongs to martensite with the orientation I (Fig. 6, *c*), and the second one — with the orientation II (Fig. 6, *d*). Fig. 7 presents electron-diffraction patterns obtained from the areas distinguished by the aperture and belonging to each orientation. Inside the plate I there is striped contrast, which is perpendicular to the rows of reflexes splitting on the electron-diffusion pattern.

In dark-field image (Fig. 6, *e*) made in azimuth fuzzy reflex belonging to the $L2_1$ lattice of austenite (in electron-diffraction pattern Fig. 6, *b* designated 3), there is the third orientation of crystal — V-shaped area designated III. That residual austenite is within the plates of martensite in the form of V-shaped insert having fragmented nanodomain structure, with atoms ordered as per the type $L2_1$. The microstructure of the residual austenite constricted between two martensite phases features high internal stresses, which is indicated by azimuth fusion of the reflexes. Moreover, the azimuth fusion of reflexes may represent V-shape of the austenite phase and disorientation of the nanodomains comprising the austenite relative to each other. The fact that only austenite phase is subjected to fragmentation indicates by monocrystalline type of electron-diffraction patterns, on which there are only specific reflexes belonging exclusively to austenite phase, and tending to azimuth fusion. Reflexes with azimuth fusion are absent on the electron-diffraction patterns obtained from the areas belonging to martensite plates only (Fig. 7). Compression of residual austenite phase by martensite results in stresses and disorientation of the areas initially coherent to the matrix, which, in turn, results in azimuth fusion of the reflexes.

The peculiarities of a thin structure V-shaped foil of the alloy $Ni_{46}Mn_{41}In_{13}$ observed herein correlate with the results of the work [19], which contain the analysis of data available in publications on the impact of size of the nanocrystals of NiFeGa and TiNi alloys to the parameters of curves of their pseudoelastic and thermoelastic deformation. This analysis assumes existence of a critical size of the nanocrystal D_k, below which there is no martensite transformation in the crystal. Moreover, the work [19] provided kinetic non-linear equations for the volumetric portions of martensite and austenite, whose solution shows, that they describe the process of self-organization of transformation dislocations, as a result of which the domain structure is formed in the crystal with inter-phase boundaries.

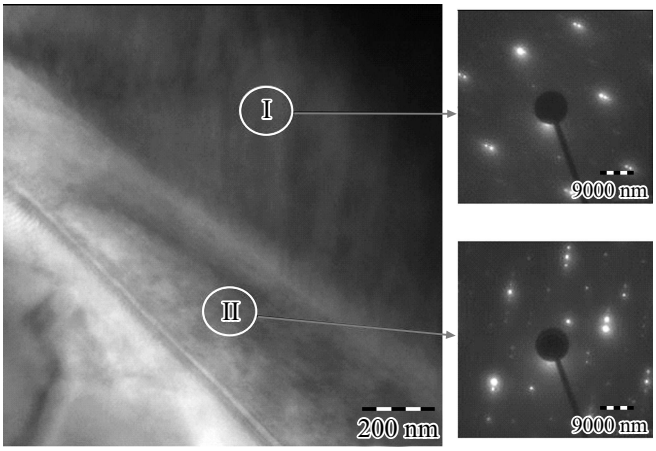

Figure 7. Light-field image of the alloy $Ni_{46}Mn_{41}In_{13}$ and electron-diffraction patterns obtained from two different orientations of the martensite.

4. Conclusion

The obtained results show, that the phase transformation in the alloy $Ni_{46}Mn_{41}In_{13}$ occurs non-uniformly all over the sample, which is indicated by versatility of the observed structures (black-white contrast, tweed, lamella structure). Below M_s the cubic $L2_1$ phase turns to modulated martensite variants with residual austenite. Further temperature reduction results in increase of the martensite phase, however, it was found that martensite transformation is completely suppressed with the plate thickness below 50 nm.

The temperatures of direct and reverse martensite transformation depend not only on the magnitude of magnetic field, but on the sample dimensions and configuration as well. Reduction of the plate thickness and magnetic fields result in decrease of the temperature of direct martensite transformation, thus expanding the area of existence of the ferromagnetic austenite.

Work funding

The research was carried out using a grant from the Russian Scientific Foundation (project No. 20-79-10197).

Conflict of interest

The authors declare that they have no conflict of interest.

References

[1] S.B. Madiligama, P. Ari-Gur, V.G. Shavrov, V.V. Koledov, S. Calder, A.V. Mashirov, A.P. Kamantsev, E.T. Dilmieva, L. Gonzalez-Legarreta, B.H. Grande, V.V. Vega, A. Kayani. Smart Mater. Structures **8**, 085013 (2016).

[2] Yu.S. Koshkid'ko, E.T. Dilmieva, J. Cwik, K. Rogacki, D. Kowalska, A.P. Kamantsev, V.V. Koledov, A.V. Mashirov, V.G. Shavrov, V.I. Valkov, A.V. Golovchan, A.P. Sivachenko, S.N. Shevyrtalov, V.V. Rodionova, I.V. Shchetinin, V. Sampath. J. Alloys Comp. **798**, 810 (2019).

[3] A.P. Kamantsev, V.V. Koledov, A.V. Mashirov, E.T. Dilmieva, V.G. Shavrov, J. Cwik, I.S. Tereshina, M.V. Lyange, V.V. Khovaylo, J. Porcari, and M. Topic. Properties of Metamagnetic Alloy $Fe_{48}Rh_{52}$ in High Magnetic Fields. Bulletin of the Russian Academy of Sciences. Physics, Vol. 79, No. 9, pp. 1086–1088 (2015). DOI: 10.3103/S1062873815090105

[4] N.I. Kourov, A.V. Korolev, V.G. Pushin, V.V. Koledov, V.G. Shavrov, V.V. Khovailo. Fizika metallov i metallovedenie (in Russian) **99**, *4*, 38 (2005).

[5] V.G. Pushin, N.I. Kourov, A.V. Korolev, V.A. Kazantsev, L.I. Yurchenko, V.V. Koledov, V.G. Shavrov, V.V. Khovailo. The Physics of Metals and Metallography Fizika metallov i metallovedenie **99**, *4*, 401 (2005).

[6] E. Kalimullina, A. Kamantsev, V. Koledov, V. Shavrov, V. Nizhankovskii, A. Irzhak, F. Albertini, S. Fabbrici, P. Ranzieri, P. Ari-Gur. Physica Status Solidi C **11**, *5–6*, 1023 (2014).

[7] A.P. Kamantsev, V.V. Koledov, A.V. Mashirov, E.T. Dilmieva, V.G. Shavrov, J. Cwik, A.S. Los, V.I. Nizhankovskii, K. Rogacki, I.S. Tereshina, Y.S. Koshkid'ko, M.V. Lyange, V.V. Khovaylo, P. Ari-Gur. J. Appl. Phys. **117**, *16*, 163903 (2015).

[8] J. Liu, Z. Liu, X. Jin. Phil. Mag. **94**, *1*, 56 (2014).

[9] V.G. Pushin, E.B. Marchenkova, A.V. Korolev, N.I. Kourov, E.S. Belosludtseva, A.V. Pushin, A.N. Uksusnikov. Physics of the Solid State **59**, *7*, 1321 (2017).

[10] S.V. Sudareva, E.I. Kuznetsova, T.P. Krinitsina, I.B. Bobylev, V.N. Morycheva, L.V. Zherdeva, E.P. Romanov. Physics of the Solid State. **75**, *2*, 199 (1993).

[11] H. Nath, G. Phanikumar. Mater. Characterization **102**, 24 (2015).

[12] Y. Ni, Y. M. Jin, A.G. Khachaturyan. Acta Mater. **55**, 4903 (2007).

[13] Y. Ni, A.G. Khachaturyan. Nature Mater. **8**, 410 (2009).

[14] Y.M. Jin, Y.U. Wang, Y. Ren. npj Comput. Mater. *1*, 15002 (2015).

[15] P. Lega, A. Kartsev, I. Nedospasov, S. Lv, X. Lv, N. Tabachkova, V. Koledov. Phys.Rev. B **101**, *21*, 214111 (2020).

[16] T. Waitz, T. Antretter, F.D. Fischer, N.K. Simha. J. Mech. Phys. Solids **55**, 419 (2007).

[17] Y.Q. Fu, S. Zhang, M.J. Wu, W.M. Huang, H.J. Du, J.K. Luo, A.J. Flewitt, W.I. Milne. Thin Solid Films **515**, 80 (2006).

[18] S.V. Sudareva, E.P. Romanov, T.P. Krinitsina, Yu.V. Blinova, E.I. Kuznetsova. The Physics of Metals and Metallography **102**, *2*, 205 (2006). DOI: 10.1134/S0031918X06080126.

[19] G.A. Malygin. Physics of the Solid State **61**, *2*, 149 (2019). DOI: 10.1134/S1063783419020173